Electrical, thermal, and species transport properties of liquid eutectic Ga-In and Ga-In-Sn from first principles

Seungho Yu and Massoud Kaviany[a)]
Department of Mechanical Engineering, University of Michigan, Ann Arbor, Michigan 48109, USA

(Received 17 December 2013; accepted 27 January 2014; published online 11 February 2014)

Using *ab initio* molecular dynamics, the atomic structure and transport properties of eutectic Ga-In and Ga-In-Sn are investigated. The Kubo-Greenwood (K-G) and the Ziman-Faber (Z-F) formulations and the Wiedemann-Franz (W-F) law are used for the electrical and electronic thermal conductivity. The species diffusivity and the viscosity are also predicted using the mean square displacement and the Stokes-Einstein (S-E) relation. Alloying Ga causes more disordered structure, i.e., broadening the atomic distance near the In and Sn atoms, which reduces the transport properties and the melting temperature. The K-G treatment shows excellent agreement with the experimental results while Z-F treatment formula slightly overestimates the electrical conductivity. The predicted thermal conductivity also shows good agreement with the experiments. The species diffusivity and the viscosity are slightly reduced by the alloying of Ga with In and Sn atoms. Good agreements are found with available experimental results and new predicted transport-property results are provided. © *2014 AIP Publishing LLC*. [http://dx.doi.org/10.1063/1.4865105]

I. INTRODUCTION

Low-meting temperature liquid metal alloys have received attention for use in the deformable electronics, electromicrofluidic systems, and thermal management. While mercury has the lowest melting temperature among elemental metals, its high surface energy and toxicity have led to the Ga alloys as replacement. Their properties include low vapor pressure, high boiling temperature, low dissolution in water, and high electrical and thermal conductivity.[1] Eutectic gallium-indium (EGaIn, $Ga_{0.858}In_{0.142}$ by atomic fraction) and eutectic gallium-indium-tin (EGaInSn, $Ga_{0.772}In_{0.143}Sn_{0.085}$) have low melting temperatures of 288.65 K (15.5 °C) and 283.65 K (10.5 °C), respectively. They have been used for stretchable antennas,[2,3] soft electrodes for molecular junctions,[4,5] microelectrodes,[6] and as liquid coolants.[7,8] However, data on the transport properties of the liquid Ga alloys are scarce and not consistent. For EGaIn, while the liquid electrical conductivity of 3.4×10^6 (ohm m)$^{-1}$ at 295 K has been reported,[9,10] there are no results at other temperatures and similarly for the single reported liquid thermal conductivity of 40 W/m K.[11] For EGaInSn, the temperature-dependent electrical conductivity is available,[12,13] but the thermal conductivity is only reported at 368 K as 39 W/m K[14] and no data for near the room temperature. Therefore, it is timely to provide the temperature-dependent transport properties of liquid Ga alloys.

Here, the transport properties of the liquid Ga, EGaIn, and EGaInSn were investigated using first-principles calculations. With the *ab initio* molecular dynamics (AIMD), the electrical, thermal, and species transport properties are predicted at near the room temperature. We also explore the atomic structures of these liquid alloys influencing their transport properties. Their structures are scrutinized through the structure factor, $S(\kappa)$, and pair correlation function, $g(r)$, which provide the atomic distribution, average distance, and medium-range order. The charge density distributions of the alloys are also investigated. The Kubo-Greenwood (K-G)[15,16] and the Ziman-Faber (Z-F)[17,18] formulations are used for the liquid electrical and electronic thermal conductivity. The total thermal conductivity is found by adding the molecular liquid thermal conductivity. The liquid species diffusivity and the viscosity are also predicted using the mean-square-displacement (MSD) and the Stokes-Einstein relation.

II. METHODS

A. AIMD simulations

AIMD calculations were performed for liquid Ga, EGaIn, and EGaInSn at various temperatures using the *Vienna Ab initio Simulation Package* (VASP) code,[19] which applies the Born-Oppenheimer approximation and the Verlet algorithm. The pseudopotentials were generated by the projector augmented wave (PAW) formalism[20,21] and the generalized gradient approximation of Perdew-Burke-Ernzerhof functional (GGA-PBE)[22] was used for the exchange-correlation potential. The electron orbitals were represented by the plane waves up to an energy cutoff of 170 eV and only the Γ point is used for the representation of the Brillouin zone. For large supercells (more than 100 atoms, such as those in this study), only when using the gamma-point, there would be converged results.

The structures of the liquid Ga, EGaIn, and EGaInSn were prepared in a cube with the periodic boundary conditions. The size of the cube was determined with the experimental density at each temperature. We used both the 128-atoms and 250-atoms supercells, in the AIMD simulations. The results from the 128-atoms cell gave transport

a)Electronic mail: kaviany@umich.edu

TABLE I. The atomic fraction used in the simulation of liquid Ga, EGaIn, and EGaInSn. The atomic volumes at each temperature found from the experimental density[14,33,34] are also listed.

			V_a (Å^3/atom)		
	N_i	Composition	310 K	335	360
Ga	250	100	19.013	19.072	19.131
EGaIn	215:35	86:14	20.112	20.195	20.272
EGaInSn	193:36:21	77.2:14.4:8.4	20.988	21.025	21.064

properties in more agreement with the experimental results. Therefore, we used 128-atoms cells in the AIMD simulations and the electronic calculations. The 250-atom cells predicted slightly more accurate results for the structural factor. So, we used the 250-atom cells for the structural behavior. The atomic ratio and the volume of each structure are summarized in Table I. Constant temperature simulations were performed in the *NVT* ensemble using a Nosé-Hoover thermostat[23] for 10 ps with time step of 1 fs. We collected the AIMD results after reaching equilibrium (elapsed time of 5 ps), and found the linear relation of the MSD of atoms with respect to time which indicates the system is in the liquid state.

B. Electrical conductivity treatments

The electrical conductivity is obtained using the K-G formulation with the *ABINIT* code[24,25] and the atomic configurations (snap shots) from the AIMD results as input. This formulation allows for directly calculating the electronic transport properties, including the ionic and the electronic scattering. For the electronic calculation, we collected five snap shots every 1 ps, after reaching equilibrium (5 ps) from the AIMD results with 128-atoms. The self-consistent, ground-state calculations were performed to obtain the electronic structure with the PAW potentials and the GGA-PBE. The energy cutoff of 243 eV and a 2 × 2 × 2 Monkhorst-Pack κ-point grid were used for the electronic calculations, and the electronics levels were occupied with the Fermi-Dirac smearing factor. The width for the Fermi-Dirac smearing is the physical temperature in the AIMD simulations.

In the K-G formulation, the electrical conductivity is[15,16]

$$\sigma_e = \frac{he_c^2}{V_c}\sum_{\kappa',\kappa}\lim_{E\to 0}\frac{f(E_{\kappa'})-f(E_\kappa)}{E} \times \delta(E_{\kappa'}-E_\kappa-E)\langle\psi_\kappa|\hat{\mathbf{v}}|\psi_{\kappa'}\rangle\langle\psi_{\kappa'}|\hat{\mathbf{v}}|\psi_\kappa\rangle, \quad (1)$$

where h is the Planck constant, e_c is the electron charge, V_c is the volume of the simulation cell, E_κ is the electronic eigenvalues, $f(E_\kappa)$ is the Fermi-Dirac occupation of eigenstate κ, ψ_κ is the wave function, and $\langle\psi_\kappa|\hat{\mathbf{v}}|\psi_{\kappa'}\rangle$ is the velocity matrix elements with the velocity operator given by the Hamiltonian gradient as

$$\mathbf{v} = \frac{i}{\hbar}[\mathrm{H},\mathbf{r}] = \frac{1}{\hbar}\frac{\partial \mathrm{H}}{\partial \boldsymbol{\kappa}}. \quad (2)$$

We used a small, finite E, i.e., 0.27 meV, which showed good convergence for the electrical conductivity results.

The electrical conductivity is also calculated with the Z-F formulation,[17,18] which assumes that the conduction electrons form a degenerate free-electron gas and are scattered by the ions with appropriate pseudopotentials in the liquid metal.[26] The elastic scattering is related to the relaxation time approximation in the Boltzmann transport equation. The electrical resistivity is calculated with the classical relation and the relaxation time τ_e[17,18]

$$\rho_e = \frac{m_e}{n_e e_c^2 \tau_e} = \frac{3\pi m_e^2 V_a}{e_c^2\hbar^3\kappa_\mathrm{F}^2}\langle|\varphi(\kappa)|^2 S(\kappa)\rangle = \frac{3\pi m_e^2 V_a}{e_c^2\hbar^3\kappa_\mathrm{F}^2}\frac{1}{4\kappa_\mathrm{F}^4}\int_0^{2\kappa_\mathrm{F}}|\varphi(\kappa)|^2 S(\kappa)\kappa^3 d\kappa, \quad (3)$$

where $\rho_e = \sigma_e^{-1}$ is the electrical resistivity, n_e is the total number of free electrons per unit volume, m_e is the mass of electron, V_a is the volume per atom, κ_F is the Fermi wave vector, $\varphi(\kappa)$ is the pseudopotential, and $S(\kappa)$ is the structure factor. The value of κ_F is obtained from $\kappa_\mathrm{F} = (3\pi^2 z/V)^{1/3}$, where z is the valency and z/V_a is the average valence electron density. For the pseudopotential, we used the optimized model potential in Ref. 27, provided in Ref. 28 and normalized to $-2/3E_\mathrm{F}$ at $\kappa = 0$. The electrical resistivity for a binary liquid alloy is calculated for EGaIn alloy using[29]

$$\rho_e = \frac{3\pi m_e^2 V_a}{e_c^2\hbar^3\kappa_\mathrm{F}^2}\frac{1}{4\kappa_\mathrm{F}^4}\int_0^{2\kappa_\mathrm{F}}[x_1\varphi_1^2(\kappa)S_{11}(\kappa) + 2(x_1x_2)^{1/2}\varphi_1(\kappa)\varphi_2(\kappa)S_{12}(\kappa) + x_2\varphi_2^2(\kappa)S_{22}(\kappa)]\kappa^3 d\kappa, \quad (4)$$

where x_i is the concentration and $S_{ij}(\kappa)$ is the partial structure factor.

C. Thermal conductivity treatments

The electronic thermal conductivity can be deduced using the Wiedemann-Franz (W-F) law and the metal Lorenz number, N_L, i.e.,

$$k_e = \sigma_e N_\mathrm{L} T. \quad (5)$$

For the liquid metals, the total thermal conductivity of k_t is the sum of k_e and the molecular liquid thermal conductivity, k_f. The Bridgman theory[30] has been widely used for the calculations of k_f with analogy of the liquid as a lattice. The thermal energy transfer by interacting particles uses the speed of sound, i.e.,

$$k_f = \frac{3k_\mathrm{B}a_s}{l^2}, \quad (6)$$

where k_B is the Boltzmann constant, a_s is the speed of sound, and l is the distance between the atoms, and is

$$l = (V_m/n_f N_\mathrm{A})^{1/3}, \quad (7)$$

where V_m is the molar volume, N_A is the Avogadro number, and n_f is the number density of atoms. In Ref. 31, a slightly modified version of Eq. (6) is used including the Eucken correction factor, to account for the internal degrees of freedom by changing the factor 3 to $2.793(c_p/c_v)$, where c_p and c_v are

specific heat at constant pressure and volume. With the Bridgman theory, the fluid-particle thermal conductivity is

$$k_f = \frac{1}{3}\rho_f c_v a_s n_f^{-1/3} = \rho_f \frac{R_g}{M} a_s \left(\frac{M}{\rho_f N_A}\right)^{1/3}, \quad (8)$$

where ρ_f is the density of the liquid, R_g is the universal gas constant, and M is the molecular weight. Assuming rigid spheres, the heat capacity is $Mc_v = 3R_g$. Rearranging k_f using the isothermal compressibility κ_f, we have

$$k_f = \frac{3R_g}{N_A^{1/3}} \frac{\rho_f^{1/6}}{M^{2/3}} \left(\frac{c_p}{c_v}\frac{1}{\kappa_f}\right)^{1/2}, \ \kappa_f = \left(\frac{1}{\rho_f}\frac{\partial \rho_f}{\partial p}\right)_T. \quad (9)$$

D. Diffusivity and viscosity treatments

The viscosity is determined using the Stokes-Einstein (S-E) relation

$$\mu = \frac{k_B T}{C R_{S-E} D}, \quad (10)$$

where C is a numerical constant, R_{S-E} is the effective radius of the diffusing particles, and D is the diffusivity calculated using the MSD as

$$D_i = \frac{\langle [\boldsymbol{x}_i(t) - \boldsymbol{x}_i(0)]^2 \rangle^o}{6t}, \quad (11)$$

where the bracket is the average over the particles with position at $\boldsymbol{x}$ and at time t, i denotes the atoms of Ga, In, and Sn, and superscript o indicates equilibrium state. We use average diffusivity and the first maximum in the $g(r)$ for R_{S-E}. In Eq. (10), C is 4π for the slipping boundary condition and 6π for the sticking boundary conditions. In Ref. 32, the relation between the diffusivity and viscosity is given as

$$(D\mu/k_B T)R_{S-E} = 0.0329(2 + \mu/\mu_l) = 1/C', \quad (12)$$

where the ratio of shear viscosity to the longitudinal viscosity μ/μ_l can be estimated based on the bulk viscosity $\mu_v = \mu/3$ and $\mu_l = 4\mu/3 + \mu_v$. This results in $C' = 11.70$ show good agreement with experiments.

III. ATOMIC STRUCTURE

The AIMD simulations were performed to investigate the effects of alloying Ga with In and Sn on the transport properties. To validate the simulation, the predicted structure factor $S(\kappa)$ for Ga is compared with the experimental results,[35] as shown in Fig. 1. The comparison between the predicted $S(\kappa)$ at 310 K and those measured at 293 K shows good agreement, which validates the AIMD simulations. The experimental results $S(\kappa)$ of Ga[36] and EGaIn[37] also show good agreements with the predicted results. The values of κ at the first peak are nearly the same for all the three compounds and there is a shoulder at the first peak. We also verified the liquid behavior of the model system from the linear temporal variation of MSD.

Figure 2 shows the predicted pair-correlation function $g(r)$ for the liquid Ga, EGaIn, and EGaInSn at 310 K and for Ga also at 500 K. The variations of $g(r)$ indicate the average

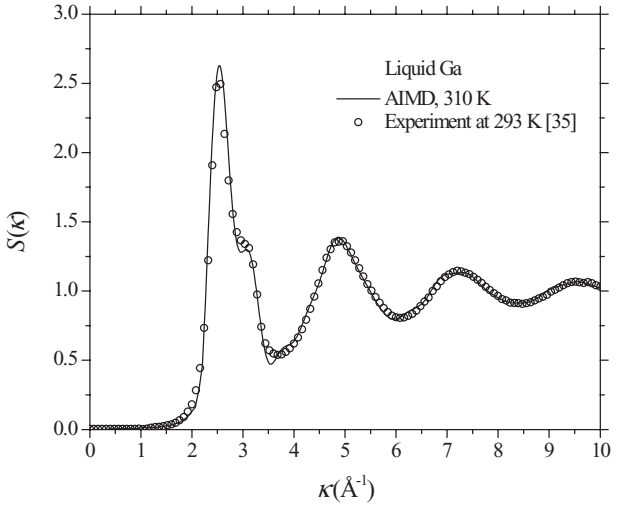

FIG. 1. The predicted structure factor of the liquid Ga at 310 K (solid line) compared with the experimental result at 293 K.[35] There is a shoulder on the right of the first peak.

probability of location atoms at a given distance r from the center of the designated atom. Figure 2 shows a first strong peak and then weaker peaks with increased distance. This explains the strong interactions in the first shell and lack of long-range order. In Fig. 2, alloying Ga with In and Sn leads to a decrease in the height of the first peak and shift of the $g(r)$ to the right, which indicates the atoms in that coordination shells are further distributed and also shows the average distance between atoms.

We compared this alloying result with the high-temperature behavior of the liquid Ga. As temperature increases, the first peak position in $g(r)$ is expected to shift to larger distance, due to thermal expansion, same as alloying with In and Sn. However, the first peak in $g(r)$ at 500 K shifts to a smaller distance, because of the decrease in the distance between atoms in the first shell. In Ref. 38, it is reported that this abnormal decrease in the inter-atomic distance is caused

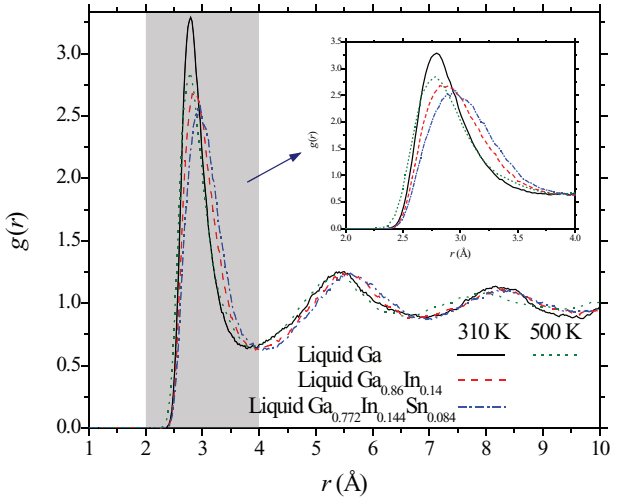

FIG. 2. Predicted pair correlation function for liquid Ga, EGaIn, and EGaInSn at 310 K and for Ga also at 500 K. The inset shows the results up $r = 4$ Å.

by the redistribution of the polyhedral clusters. They show that this phenomenon is a general feature for the metallic melts consisting of various-size polyhedrals. Therefore, the high-temperature structural behavior is different than the alloying effect which shifts the first peak in $g(r)$ to the right. Alloying with In and Sn increases the average distance in the first shell caused in the disordered structure compared to the redistribution of the polyhedral clusters. The lower and broad peaks in EGaIn and EGaInSn also show the disordered structure of the liquid alloys.

Due to the larger atomic volume of the In and Sn, progressively displacing extra Ga atoms with In and Sn gradually shifts the first peak position to the right and increases the atomic volume. The first peak in $g(r)$ and the volume per atom continuously increase to 2.785, 2.874, 2.958 Å, and 19.01, 20.11, 20.99 Å^3/atom for Ga, EGaIn, and EGaInSn, respectively. To further investigate the effect of each atom on the increase in $g(r)$ and the atomic volume, the partial pair-distributions functions, $g_i(r)$, for EGaInSn at 310 K are calculated and shown in Fig. 3. For the $g_i(r)$ between Ga atoms, the minimum distance is 2.41 Å and the first peak is similar to the $g(r)$ in Fig. 2, which indicates the force field among Ga atoms does not change significantly. The minimum distance between Ga and other elements increases to 2.58 Å, and the first peak shifts to the right. With In and Sn alloying of Ga, their larger atomic volume leads to the disordered structure by expanding the cell volume and broadening their inter-atomic distance.

Figure 4 is the predicted $S(\kappa)$ for liquid Ga, EGaIn, and EGaInSn at 310 K and for Ga also at 500 K. The $S(\kappa)$ results are obtained using the Fourier transform of the $g(r)$ with the ISAACS program.[39] Alloying with In and Sn leads to decrease in the height of the first peak and shifts the $S(\kappa)$ to the left. The first peak is related to the medium-range structure order corresponding to the structure in the 2nd and higher coordination shells in $g(r)$. Therefore, the reduced height denotes disordered structure of alloys, while the left shift of alloys and the right shift of Ga at 500 K illustrate increase in the average distance between atoms. These are consistent with the results for $g(r)$ discussed above. The shoulder on the high-κ side of the first peak in $S(\kappa)$ of liquid Ga is diminished by alloying with In and Sn, and by increase in the temperature. The origin of the high-κ side of the first peak in $S(\kappa)$ was explained with the short-lived covalent dimers[40] and the formation of clusters.[41] However, recent studies[42,43] question these and propose a modulation on the local structures caused by the Friedel oscillations, which are mainly determined by the soft repulsive core. Alloying with In and Sn, and increase in the temperature causes the weakening of this Friedel oscillation, which reduces the modulation and cause the disappearance of the shoulder.

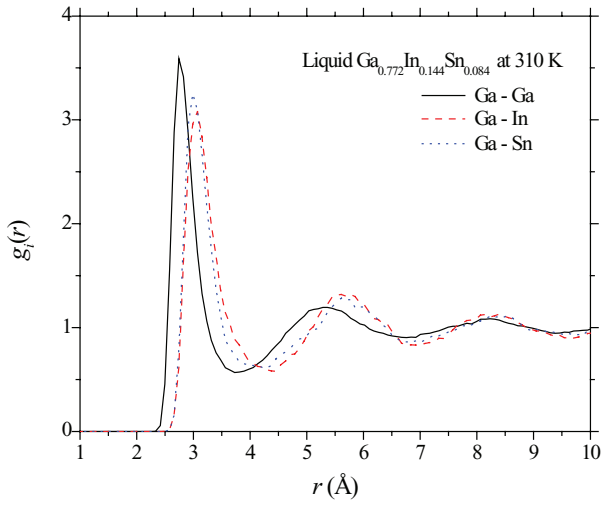

FIG. 3. Predicted partial radial distribution function, $g_i(r)$ for liquid EGaInSn at 310 K.

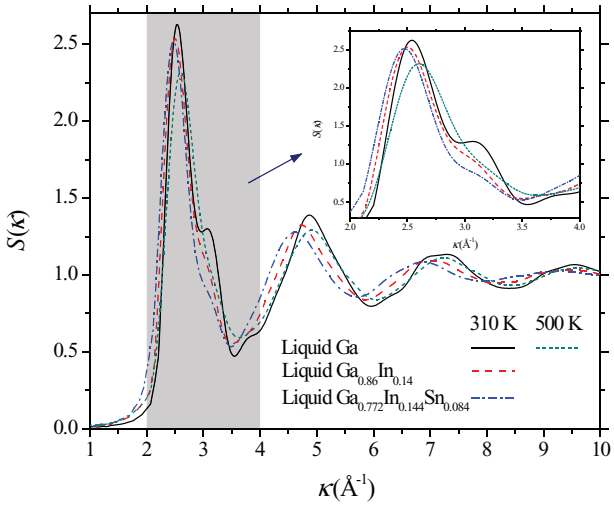

FIG. 4. Predicted structure factors for liquid Ga, EGaIn, and EGaInSn at 310 K, and for Ga also at 500 K. The inset shows the results for $\kappa = 4$ Å^{-1}.

The constant charge density contours for EGaInSn at 310 K are obtained from the snap shots of the AIMD results, and shown in Fig. 5(a). Using VESTA,[44] the charge density contours are presented with intervals of 0.005 e_cÅ^{-3}, from 0 (blue) to 0.038 (red) e_cÅ^{-3}. The high-charge density between Ga atoms represents the valence electron for the given atomic configuration. In Ref. 43, the existence of Ga_2 dimers is questioned, since their bonds are very short-lived in the liquid Ga and the dimers vibrational mode is not found. In Fig. 5(a), the charge density is higher between Ga atoms, which indicates strong force field among Ga atoms (while In and Sn have weaker interactions). Moreover, the charge density near the In atoms is significantly smaller compared to Sn atoms which tightly hold the electrons. This feature of the In atoms can explain the dominant role of In in reducing the electrical transport properties.

The electron distribution near the In and Sn atoms is comparable to that for Hg, where the electrons in the low-energy orbitals are very strongly bound to the atom similar to the weak interacting noble-gas atoms, which result in low melting temperature (234.3 K for Hg).[45] This behavior of the In and Sn atoms explains the low-melting point of EGaIn (288.65 K) and EGaInSn (283.65 K) compared to Ga (303 K). Figure 5(b) shows the structure of the liquid EGaInSn at 310 K with the iso-surface charge density of 0.035 e_cÅ^{-3}. The bonding indicates that the distance between the atoms is less than 2.65 Å, i.e., only Ga bonds are found. As discussed in Fig. 3, the inter-atomic distance involving the In and Sn atoms

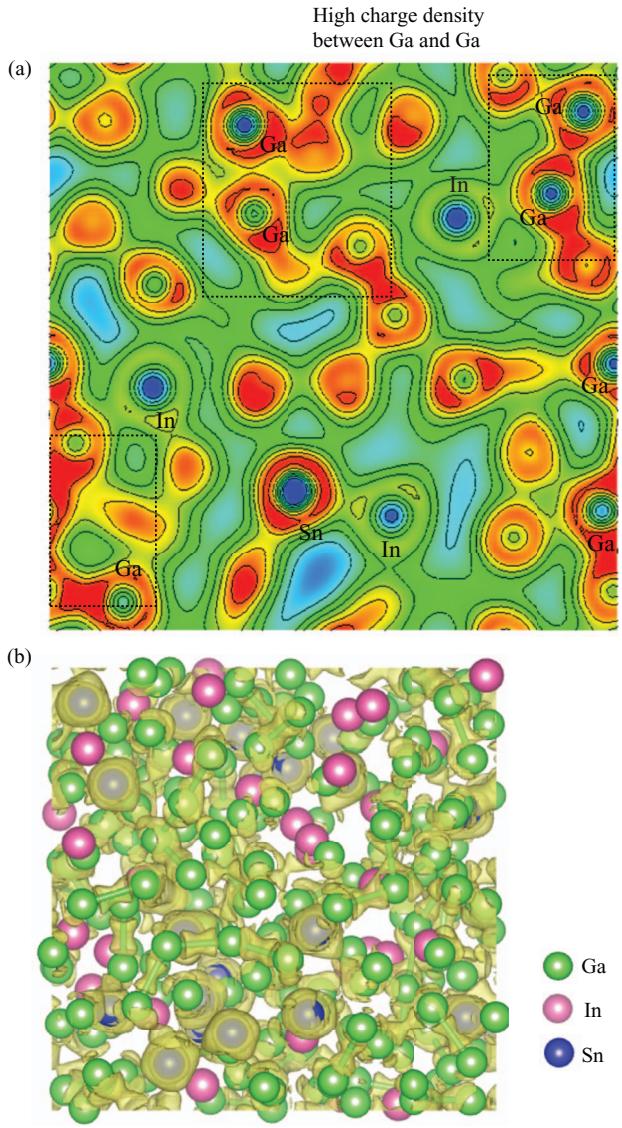

FIG. 5. (a) Contours of charge densities for liquid EGaInSn at 310 K, from 0 (blue) to 0.038 (red) e_cÅ^{-3}. (b) Structure of the liquid EGaInSn at 310 K with contours of the constant charge density of 0.035 e_cÅ^{-3}. Bonds indicate the length between the atoms is less than 2.65 Å.

are larger, while Ga atoms maintain their bonds. The iso-surface charge density in Fig. 5(b) is the three-dimensional version of Fig. 5(a), which clearly illustrates the weak interaction of the In and Sn atoms.

IV. ELECTRICAL CONDUCTIVITY

The electrical conductivity σ_e of the liquid Ga, EGaIn, and EGaInSn are predicted as a function of temperature and shown in Fig. 6. The Z-F formula overestimates the σ_e of Ga and EGaIn compared to the experimental results. Due to the limited number of atoms in the AIMD simulations, $S(\kappa)$ has uncertainties associated with representing the exact medium-range structure order corresponding to the higher-coordination shells. Since the Z-F formula predicts the σ_e using the $S(\kappa)$ for the range of $\kappa \leq 2\kappa_F$ (the first peak), this uncertainties cause slightly higher σ_e for the liquid Ga. The larger overestimation of σ_e for the liquid EGaIn is caused by

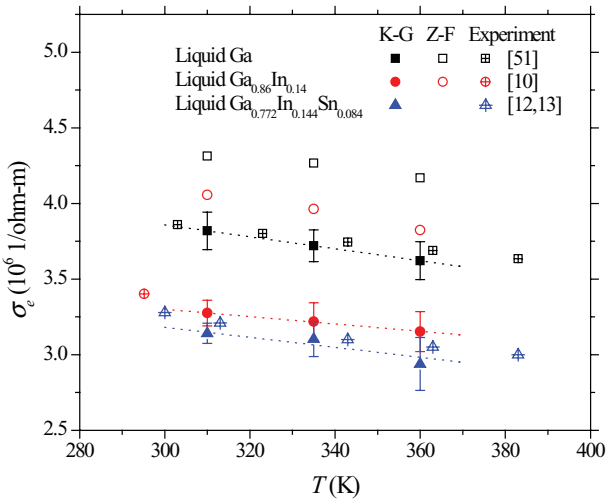

FIG. 6. The predicted variations of the electrical conductivity of the liquid Ga, EGaIn, and EGaInSn with respect to temperature using the K-G and the Z-F treatments and comparison with the experimental results.[25,46–50] The dashed lines are linear fits for the results from the K-G treatments.

the smaller number of In atoms (14), which influences the accuracy of the partial structure factors $S_{12}(\kappa)$ and $S_{22}(\kappa)$ used in Eq. (4). In addition, the Z-F theory is the simplest approach to the electrical transport and does not include the multiple scattering effects. Moreover, the pseudopotential of the optimized model potential[27,28] also overestimates the effective mass and the exchange-correlation corrections which cause an increase in the σ_e for liquid Ga.[26]

The K-G treatment has been generally used to obtain σ_e using the *ab initio* simulations[25,46–50] and σ_e is directly obtained with the self-consistent calculations using the electronic excitation structure, which includes ionic and electronic scattering. This K-G treatment overcomes the weak-scattering limit of the Z-F treatment. In Fig. 6, the results of σ_e obtained from the K-G treatment show very good agreement with the experimental results.[10,12,13,51] The average values from five snap shots and the standard deviations are presented with a linear fit to the result. The values of σ_e decrease to 3.28 and 3.14 $\times$ 10^6 (ohm m)$^{-1}$ at 310 K for EGaIn, and EGaInSn, compared to 3.82 $\times 10^6$ (ohm m)$^{-1}$ for Ga, corresponding to a 14.1% and 17.8% decrease. As mentioned in Fig. 5, this decrease is due to the role of In and Sn atom causing disordered structures as well as weak inter-atomic interactions. The larger decrease in σ_e between Ga and EGaIn in Fig. 6 indicates that the very low charge density near the In atoms contributes significantly to the reduction in the electrical conductivity.

V. THERMAL CONDUCTIVITY

The variations of the predicted thermal conductivities of liquid Ga, EGaIn, and EGaInSn with respect to temperature are shown in Fig. 7, along with comparison with the experimental results for Ga.[52] The magnitude of k_t is the sum of k_e and k_f, from Eqs. (5) and (9). We predict k_e using Eq. (5) since k_e is directly related to σ_e through the W-F law. The metallic Lorenz number $N_L = 2.44 \times 10^{-8}$ W ohm K^{-2} has already

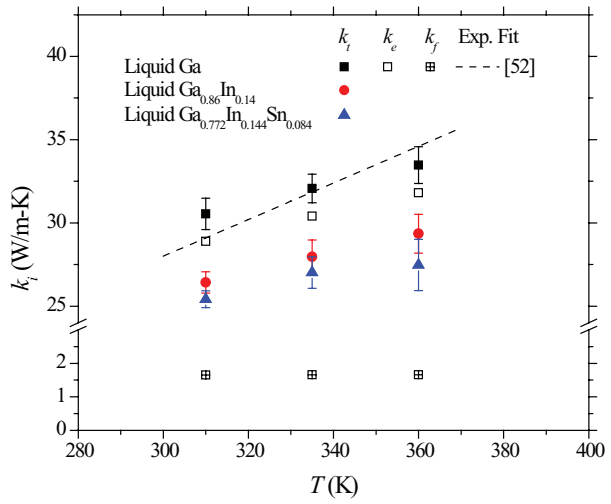

FIG. 7. The predicted variations of the total thermal conductivity of the liquid Ga, EGaIn, and EGaInSn with temperature and comparison with the experimental results.[52] The dashed line is the linear fit for to the experimental thermal conductivity of liquid Ga from five different sources.

been confirmed in the temperature range of 293.3–348.3 K.[53] The value of k_t for Ga shows good agreement with the dashed line fitted to five experiments.[52]

The value of k_f is about 1.65 W/m-K for Ga and nearly temperature dependent. This value is higher compared to typical nonmetallic liquids, because of the high speed of sound and the low compressibility of the liquid metals.[54] The speed of sound and the compressibility are 2740 and 1057 m/s, and 2.20×10^{-11} and 44.6×10^{-11} Pa^{-1} for Ga at 303 K and water at 300 K, respectively. Here, k_f for liquid EGaIn and EGaInSn are assumed to be same as that for liquid Ga, since k_f is expected to be dominated by the Ga-Ga interations. Figure 7 shows the reliable values of k_t for Ga, EGaIn, and EGaInSn with the range of 25–33 W/m K near the room temperature. The lower values of k_t for EGaIn, and EGaInSn are consistent with the experimental results for σ_e.

Since the k_e dominates the k_t of liquid Ga, EGaIn, and EGaInSn, the effect of alloying with In and Sn on k_t follows the interpretation of the σ_e. The decrease in the electron mean free paths reduces k_e of EGaIn and EGaInSn. The electron mean free paths, λ_e is[55]

$$\lambda_e = \frac{3k_e}{n_{e,c}c_{v,e}u_F} = \frac{3k_e}{n_{e,c}(\pi^2 k_B^2 T/2E_F)(2E_F/m_e)^{1/2}}, \quad (13)$$

where $n_{e,c}$ is the number of conduction electrons, E_F is the Fermi energy, and u_F is the Fermi velocity. In Table II, the values of λ_e are listed and decrease to 14.85 Å and 14.28 Å for EGaIn and EGaInSn compared to 16.90 Å for Ga, at 310 K. This presents the more disordered structure of the liquid EGaIn and EGaInSn which impedes the electron transport, resulting in decrease in the electrical and thermal transport.

VI. DIFFUSIVITY AND VISCOSITY

The species transport properties and the viscosity of liquid Ga, EGaIn, and EGaInSn are also predicted using the AIMD results. Figures 8 and 9(a) show the variations of species diffusivity D obtained from the MSD relations and the viscosity μ derived by the S-E formula with respect to temperature. In Fig. 8, the D for alloys are calculated by averaging the self-diffusivity for each atom obtained from the MSD and then using Eq. (11). The predicted species diffusivity of the liquid Ga is in good agreement with experimental results[56] and diffusivities of liquid EGaIn and EGaInSn are nearly the same compared to Ga. This is expected since the D of In and Sn are only slightly smaller than Ga.[57] The viscosity of liquid Ga, EGaIn, and EGaInSn are predicted using these diffusivities and the effective radius, R_{S-E}. In Fig. 9(a), The viscosity of EGaIn and EGaInSn are also slightly reduced due to the increase in R_{S-E}. While the value of the viscosity is reasonable, it is nearly independent of temperature and the atomic substitutions when compared to experimental results.[14,58–60] This is because we use a constant R_{S-E} from the first peak in $g(r)$ (nearly constant with temperature and atomic substitutions).

Figure 9(b) shows the variations of empirical R_{S-E} with respect to temperature derived using Eq. (10) with the experimental results for viscosity for Ga. While R_{S-E} from V_a and $g(r)$ are nearly independent of temperature, the empirical R_{S-E} shows a relatively strong temperature dependence. An empirical relation has been proposed in place of Eq. (10) and is[61–63]

$$D\mu^a = \text{constant}, \quad (14)$$

where a is a fitting parameter ranging from 0.62 to 1.56. Applying $a = 0.68$ in Ref. 61 and using R_{S-E} from $g(r)$, the

TABLE II. Properties of liquid Ga, EGaIn, and EGaInSn at 310 K. E_F and k_e are obtained using the AIMD results.

	E_F (eV)	$n_{e,c}$ (10^{28} m^{-3})	u_F (10^6 m/s)	$c_{v,e}$ (10^{-25} J/K)	k_e (W/m K)	λ_e (Å)
Ga	10.648	15.757	1.934	1.709	30.54	16.90
EGaIn	10.256	14.896	1.898	1.775	26.43	14.85
EGaInSn	10.154	14.673	1.889	1.793	25.41	14.28

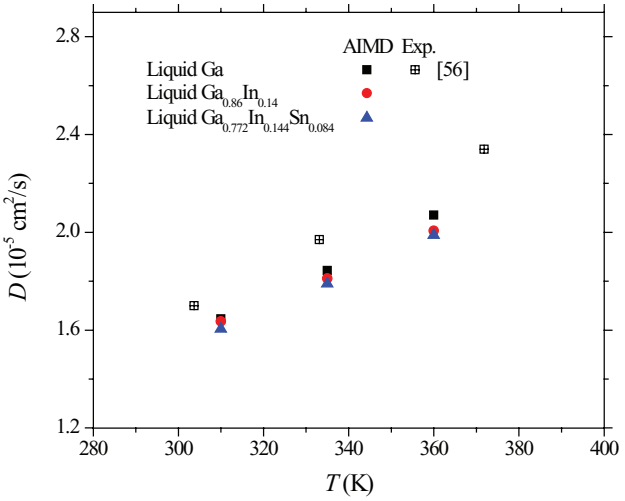

FIG. 8. The predicted variations of the species diffusivity of liquid Ga, EGaIn, and EGaInSn with respect to temperature, obtained from the MSD and comparison with the experimental result for liquid Ga.[56]

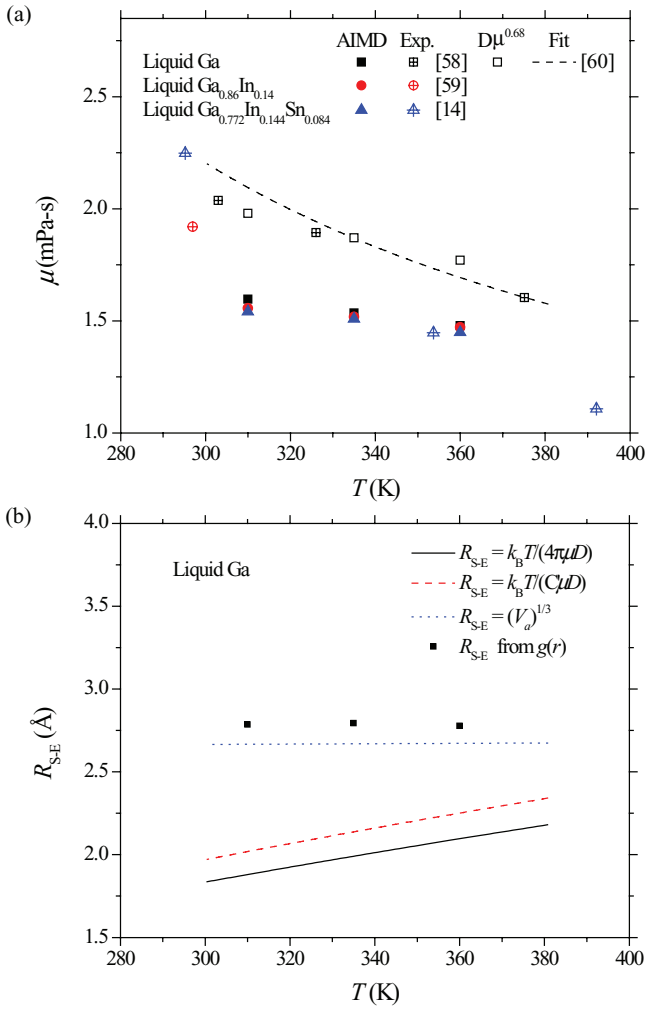

FIG. 9. (a) The variations of predicted viscosity of liquid Ga, EGaIn, EGaInSn with temperature, obtained from the S-E formula with nearly temperature-independent R_{S-E} and comparison with the experimental results[14,58,59] and the analytical relation.[60] (b) Comparison of the predicted variations of effective radius with respect to temperature, deduced from the S-E relation and the experimental results for viscosity, and those from the AIMD results for the atomic volume and for $g(r)$.

viscosity of liquid Ga becomes 1.98, 1.87, and 1.77 mPa s at 310, 335, and 360 K, respectively. This relation also shown in Fig. 9(a) is in good agreement with the experimental results near the room temperature.

VII. CONCLUSIONS

The effects of alloying Ga with In and Sn on the atomic structure and transport properties of liquid EGaIn and EGaInSn were investigated using the AIMD simulations. Alloying with In and Sn causes more disordered structure around In and Sn atoms by broadening the inter-atomic distance, while the Ga atoms nearly maintain their structure. Alloying with In and Sn also leads to the weak interaction near those atoms as illustrated in the charge density distribution. This leads to decrease in the magnitude of the σ_e and the melting temperature. The K-G treatment of the liquid electrical conduction shows excellent agreement with the experimental results, while the Z-F treatment slightly overestimates the σ_e. The larger decrease in σ_e of EGaIn was explained by the weaker interaction of the In atoms. The predicted k_t for liquid Ga also shows good agreement with the experiments, indicating the validity of the W-F law. The decreases in the σ_e and k_e were caused by the further disordered structure which reduces the magnitude of λ_e of EGaIn and EGaInSn. The D and μ were slightly lowered by the alloying of Ga with In and Sn atoms. The predicted μ presented a weak function of temperature and atomic substitutions when using a constant R_{S-E}, and we show the temperature and concentration dependence of empirical R_{S-E}. In conclusion, we elucidated the effects of alloying the liquid Ga and provided new transport properties for the liquid EGaIn and EGaInSn.

ACKNOWLEDGMENTS

We are grateful for the support of the National Science Foundation (NSF), through Grant No. CBET 1332807.

[1] K. Q. Ma and J. Liu, Front. Energy Power Eng. China **1**, 384 (2007).
[2] X. Cheng, A. Rydberg, K. Hjort, and Z. Wu, Appl. Phys. Lett. **94**, 144103 (2009).
[3] J.-H. So, J. Thelen, A. Qusba, G. J. Hayes, G. Lazzi, and M. D. Dickey, Adv. Funct. Mater. **19**, 3632 (2009).
[4] C. A. Nijhuis, W. F. Reus, and G. M. Whitesides, J. Am. Chem. Soc. **131**, 17814 (2009).
[5] M. M. Thuo, W. F. Reus, C. A. Nijhuis, J. R. Barber, C. Kim, M. D. Schulz, and G. M. Whitesides, J. Am. Chem. Soc. **133**, 2962 (2011).
[6] J.-H. So and M. D. Dickey, Lab Chip **11**, 905 (2011).
[7] A. Miner and U. Ghoshal, Appl. Phys. Lett. **85**, 506 (2004).
[8] I. Silverman, A. L. Yarin, S. N. Reznik, A. Arenshtam, D. Kijet, and A. Nagler, Int. J. Heat Mass Transfer **49**, 2782 (2006).
[9] R. C. Chiechi, E. A. Weiss, M. D. Dickey, and G. M. Whitesides, Angew. Chem., Int. Ed. **47**, 142 (2008).
[10] D. Zrnic and D. S. Swatik, J. Less-Common Met. **18**, 67 (1969).
[11] U. Ghoshal, D. Grimm, S. Ibrani, C. Johnston, and A. Miner, in *Semiconductor Thermal Measurement and Management Symposium, Twenty First Annual IEEE* (IEEE, 2005), p. 16.
[12] Ya. I. Dutchak, V. Ya. Prokhorenko, and E. A. Ratushnyak, Sov. Phys. J. **13**, 937 (1970).
[13] V. Ya. Prokhorenko, B. A. Ratushnyak, and B. P. Stadnyk, Teplofiz. Vys. Temp. **8**, 374 (1970).
[14] V. Ya. Prokhorenko, V. V. Roshchupkin, M. A. Pokrasin, S. V. Prokhorenko, and V. V. Kotov, High Temp. **38**, 954 (2000).
[15] R. Kubo, J. Phys. Soc. Jpn. **12**, 570 (1957).
[16] D. A. Greenwood, Proc. Phys. Soc., London **71**, 585 (1958).
[17] J. M. Ziman, Philos. Mag. **6**, 1013 (1961).
[18] T. E. Faber and J. M. Ziman, Philos. Mag. **11**, 153 (1965).
[19] G. Kresse and J. Furthmüller, Phys. Rev. B **54**, 11169 (1996).
[20] G. Kresse and D. Joubert, Phys. Rev. B **59**, 1758 (1999).
[21] P. E. Blöchl, Phys. Rev. B **50**, 17953 (1994).
[22] J. P. Perdew, K. Burke, and M. Ernzerhof, Phys. Rev. Lett. **77**, 3865 (1996).
[23] S. Nosé, J. Chem. Phys. **81**, 511 (1984).
[24] X. Gonze, J.-M. Beuken, R. Caracas, F. Detraux, M. Fuchs, G.-M. Rignanese, L. Sindic, M. Verstraete, G. Zerah, F. Jollet, M. Torrent, A. Roy, M. Mikami, Ph. Ghosez, J.-Y. Raty, and D. C. Allan, Comput. Mater. Sci. **25**, 478 (2002).
[25] V. Recoules and J.-P. Crocombette, Phys. Rev. B **72**, 104202 (2005).
[26] M. C. Bellissent-Funel, R. Bellissent, and G. Tourand, J. Phys. F: Met. Phys. **11**, 139 (1981).
[27] R. W. Shaw, Phys. Rev. **174**, 769 (1968).
[28] M. Appapillai and A. R. Williams, J. Phys. F: Met. Phys. **3**, 759 (1973).
[29] N. M. Ashcroft and D. C. Langreth, Phys. Rev. **155**, 682 (1967).
[30] P. W. Bridgman, *The Physics of High Pressures* (G. Bell and Sons, London, 1949).
[31] J. F. Kincaid and H. Eyring, J. Chem. Phys. **6**, 620 (1938).
[32] R. Zwanzig, J, Chem. Phys. **79**, 4507 (1983).
[33] W. H. Hoather, Proc. Phys. Soc. **48**, 699 (1936).
[34] V. V. Roshchupkin, M. A. Pokrasin, and A. I. Chernov, Zh. Fiz. Khim **LV**, 2701 (1981).

[35]A. H. Narten, J. Chem. Phys. **56**, 1185 (1972).
[36]W. Hoyer, E. Thomas, and M. Wobst, Kristall und Technik **15**, 903 (1980).
[37]K. S. Vahvaselkä, Phys. Status Solidi A **72**, 261 (1982).
[38]H. Lou, X. Wang, Q. Cao, D. Zhang, J. Zhang, T. Hu, H. Mao, and J. Jiang, Proc. Natl. Acad. Sci. U.S.A. **110**, 10068 (2013).
[39]S. Le Roux and V. Petkov, J. Appl. Cryst. **43**, 181 (2010).
[40]X. G. Gong, G. L. Chiarotti, M. Parrinello, and E. Tosatti, Europhys. Lett. **21**, 469 (1993).
[41]S.-F. Tsay and S. Wang, Phys. Rev. B **50**, 108 (1994).
[42]K. H. Tsai, T.-M. Wu, and S.-F. Tsay, J. Chem. Phys. **132**, 034502 (2010).
[43]J. Yang, J. S. Tse, and T. Iitaka, J. Chem. Phys. **135**, 044507 (2011).
[44]K. Momma and F. Izumi, J. Appl. Crystallogr. **44**, 1272 (2011).
[45]L. J. Norrby, J. Chem. Ed. **68**, 110 (1991).
[46]P. L. Silvestrelli, Phys. Rev. B **60**, 16382 (1999).
[47]F. Knider, J. Hugel, and A. V. Postnikov, J. Phys.: Condens. Matter **19**, 196105 (2007).
[48]B. Holst, M. French, and R. Redmer, Phys. Rev. B **83**, 235120 (2011).
[49]N. de Koker, G. Steinle-Neumann, and V. Vlček, Proc. Natl. Acad. Sci. U.S.A. **109**, 4070 (2012).
[50]D. V. Knyazev and P. R. Levashov, Comput. Mater. Sci. **79**, 817 (2013).
[51]M. Pokorny and H. U. Astrom, J. Phys. F: Met. Phys. **6**, 559 (1976).
[52]M. G. Braunsfurth, A. C. Braunsfurth, A. Juel, T. Mullin, and D. S. Riley, J. Fluid Mech. **342**, 295 (1997).
[53]G. Busch, H.-J. Güntherodt, and P. Wyssmann, Phys. Lett. A **39**, 89 (1972).
[54]O. J. Kleppa, J. Chem. Phys. **18**, 1331 (1950).
[55]M. Kaviany, *Heat Transfer Physics*, 2nd ed. (Cambridge University Press, New York, 2014).
[56]J. Petit and N. H. Nachtrieb, J. Chem. Phys. **24**, 1027 (1956).
[57]H. A. Walls and W. R. Upthegrove, Acta Metallurgica **12**, 461 (1964).
[58]K. E. Spells, Proc. Phys. Soc. **48**, 299 (1936).
[59]Q. Xu, E. Brown, and H. M. Jaeger, Phys. Rev. E **87**, 043012 (2013).
[60]C. J. Seeton, Tribol. Lett. **22**, 67 (2006).
[61]G. L. Pollack and J. J. Enyeart, Phys. Rev. A **31**, 980 (1985).
[62]R. Zwanzig and A. K. Harrison, J. Chem. Phys. **83**, 5861 (1985).
[63]A. S. Chauhan, R. Ravi, and R. P. Chhabra, Chem. Phys. **252**, 227 (2000).